Photoplethysmography imaging algorithm for real-time monitoring of skin perfusion maps

Uldis Rubins
University of Latvia
Raina Bulv.19, Riga LV-1586
Latvia
uldisrubins@yahoo.com

Aleksejs Miscuks
University of Latvia
Raina Bulv.19, Riga LV-1586
Latvia
aleksejsmiscuks@gmail.com

Yousef Qawqzeh
University of Fujairah
Hamad Bin Abdullah str.
Fujairah, 1207, UAE
yousef.qawqzeh@uof.ac.ae

Zbignevs Marcinkevics
University of Latvia
Raina Bulv.19, Riga LV-1586
Latvia
zbignevs.marcinkevics@lu.lv

Andris Grabovskis
University of Latvia
Raina Bulv.19, Riga LV-1586
Latvia
andris.grabovskis@gmail.com

Abstract

Photoplethysmography imaging (PPGI) is a cost-effective and reliable contactless optical technique for assessing cutaneous microcirculation. Its applications extend beyond extracting vital signs, such as heart rate and respiratory rate, to include spatiotemporal perfusion measurements from human skin. We propose an algorithm that provides real-time estimation of perfusion maps with adequate spatial resolution (320x240 pixels) and temporal resolution (0.2 s), which can be executed on a mid-range laptop computer. The algorithm was tested for determining perfusion changes in skin regions during regional anesthesia (RA) procedures. Seven patients (aged 18-80 years) undergoing hand surgery received peripheral nerve brachial plexus blocks during RA procedures. At baseline and after the RA procedure, 4, 10, 15, and 20 minutes later, the perfusion map density showed median values of 53.7%, 57.3%, 64.3%, 70.6%, and 71.1%, respectively, indicating an increase in perfusion due to the local anesthetic. Our easy-to-implement real-time video processing algorithm demonstrates potential for skin perfusion monitoring during RA procedures.

1. Introduction

Continuous monitoring of cutaneous microcirculation (skin blood perfusion) plays a crucial role in various clinical applications, such as assessment of wounds and burns [1,2], blood flow monitoring during plastic surgeries [3], diagnosing microcirculation disease in diabetic patients [2,4], critical care [4-6], and regional anesthesia monitoring [7-12]. In recent years, there has been a growing demand for cost-effective, non-contact, and reliable techniques to assess cutaneous microcirculation in clinical settings. Photoplethysmography (PPG) imaging (PPGI) has emerged as a promising technique for this purpose [7-27]. PPGI systems, comprising a video camera and a light source (visible or NIR) positioned on the same side of the tissue surface, detect time-varying intensity modulations influenced by blood volume pulsations underneath the skin.

PPGI systems have garnered interest due to their non-contact, light-based nature. Their applications extend beyond extracting high-level vital signs, such as heart rate [13-18] and respiratory rate [17-19], to measuring spatiotemporal perfusion from the face and hands in constrained environments [7-12, 20-27]. However, PPGI systems face challenges, including the small amplitude of time-varying intensity modulations, which are strongly affected by the relative movement of the camera, light source, and body, resulting in a poor signal-to-noise ratio (SNR). To overcome motion artifacts and other challenges, considerable efforts have been dedicated to finding adequate and efficient processing methods for PPGI signals. Averaging (blurring) of video pixels is the most popular method to increase SNR [13-20]. Fourier analysis is other popular technique applied to increase SNR [24]. However, spatial resolution of blurred PPG images is too low for visualization of good quality perfusion maps, because of necessity of averaging large number of pixels for increasing SNR. Fourier analysis also does not improve SNR at longer observation times due to natural instability of the pulse rate. Recently, researchers have proposed algorithms for calculating perfusion maps with high spatial resolution [21-23]. Kamshilin et al. demonstrated enhanced resolution by computing perfusion maps using the complex inner-product between the reference signal

and signals obtained from video pixels [21]. Amerald et al. introduced a method for visualizing jugular vein pulsations on the skin using Pearson's linear correlation coefficient between finger contact PPG signals and video signals [23]. However, these complex algorithms require high computing power, making them impractical for use in clinical environments that necessitate continuous monitoring of perfusion maps.

In this article, we propose an algorithm capable of performing real-time calculations of perfusion maps with adequate resolution. Our algorithm, based on the method described in [23], is adapted for real-time calculations on a middle-range laptop computer. Compared to existing techniques, our proposed algorithm addresses the limitations and provides a more suitable solution for clinical environments. The PPGI device [10] has been tested in our laboratory and operational theater during regional anesthesia procedures. To the best of our knowledge, our proposed algorithm is the first to achieve real-time PPGI map calculations with adequate resolution.

2. Methods

The PPGI prototype device (Fig. 1) was developed in the Biophotonics Laboratory of the Institute of Atomic Physics and Spectroscopy (IAPS), University of Latvia. Designed for integration with a surgical lamp in the operating room, the PPG imaging modality comprises two components: 1) the hardware and 2) video processing software, including built-in video processing algorithms. This system is capable of detecting subtle changes in blood perfusion beneath the skin.

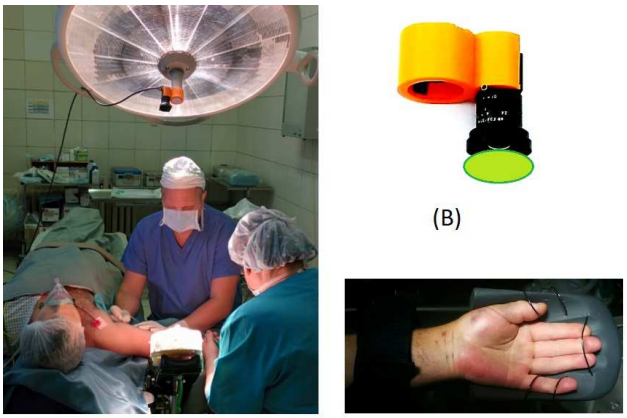

Figure 1: PPGI setup during regional anesthesia procedure (a): the camera with holder and 540nm filter (b) was attached to surgical lamp. The subject's palm was fixed to palm holder (c) to avoid the movements.

2.1. Hardware

The PPGI system utilizes a compact, lightweight industrial camera (Ximea-xiQ, CMOSIS CMV300 monochrome, 10-bit dynamic range, resolution 640x480) equipped with a low-distortion lens (Edmund Optics, C-mount f=25mm) and a 540nm CWL 10nm FWHM narrow-band filter (Edmund Optics). The camera is housed in a custom-designed 3D-printed case, which is adapted for handle attachment on the illuminator (Fig.1a). The illuminator consists of a warm-white-light surgical lamp (ALM Prismalix PRX800). To achieve a uniform illumination of an adult palm (20x15cm field of view), the lamp is positioned approximately 1.5m perpendicular to the patient's palm surface. The camera is connected to a laptop computer via a USB-3 port, which also provides power to the camera. This setup is convenient and does not obstruct the doctor-anesthesiologist or medical staff from performing their standard procedures.

2.2. Measurement procedure

The clinical measurements were conducted at the Hospital of Traumatology and Orthopedics (Riga, Latvia) under the approval of the Research Ethics Committee of the University of Latvia and in accordance with the Declaration of Helsinki. All subjects were informed about the study protocol and provided their written informed consent. Seven patients, aged 18-80 years, who were undergoing hand surgery received ultrasound-guided axillary brachial plexus blocks with peripheral nerve stimulation support.

During the recording, patients were positioned supine. The dorsal aspect of their hand was comfortably placed in a custom-made black foam rubber hand support. Room temperature was maintained at 23.0±0.5°C. The block was administered using a combination of 10 ml Sol.Lidocaini 2% and 10 ml Sol.Bupivacaini 0.5%. Following the measurement, the anesthesia level was assessed using conventional methods, such as skin touch with an ice cube.

Video recording was carried out continuously for 20 minutes during several stages of the measurement: 1) baseline (0-1 minute), 2) administration of local anesthetics (LA) (1-5 minutes), and 3) continuous monitoring after administering LA (5-20 minutes).

2.3. Video and PPGI signal processing

Real-time signal processing is crucial for continuous blood perfusion monitoring in clinical settings. Video processing encompasses video acquisition and PPG signal processing, which should be performed synchronously, with minimal time delay. The acquisition of the video stream is performed by the software with a frame rate of 25 frames and resolution 640x480 pixels. To achieve high dynamic range of PPG signals, uncompressed 10-bit

grayscale video format were chosen. The video frame rate 25 was chosen based on the fact that the frequency of the electrical network in the EU is 50 Hz, causing artificial lighting to oscillate at a frequency of 100 Hz, to prevent interference between the PPG signal and light.

The processing begins with the accumulation of video segments in a 0.2s buffer (5 frames). Further steps include: 1) spatial filtering and downsampling, 2) temporal filtering, 3) calculation of reference signal, 4) calculation of perfusion map, and 5) visualization of perfusion maps. Figure 2 demonstrates the processing pipelines described below.

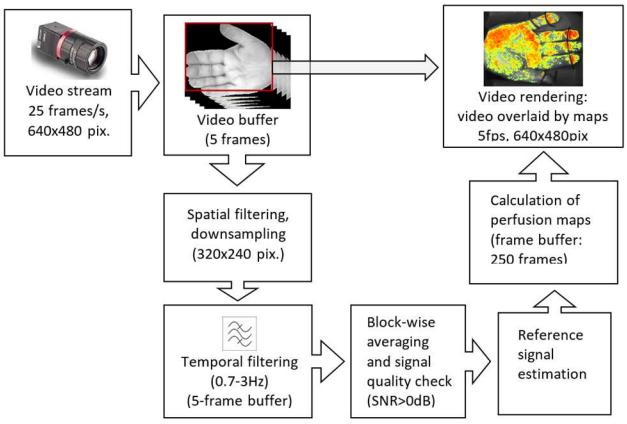

Figure 2: The real-time PPGI processing pipeline.

Spatial filtering and downsampling typically result in a significant increase in video dynamic range, essential for obtaining high-quality PPG signals from image pixels. The efficient and computationally saving method involves smoothing and downsampling each video frame using the Gaussian pyramid technique [28]. Each pixel of the smoothed image contains a local average corresponding to a pixel neighborhood on a lower level of the pyramid. Smoothed image can be expressed by the following formula:

$$G(x,y) = \sum_{m=-2}^{2}\sum_{n=-2}^{2} w_{m,n} \cdot I\left(\frac{2x+n}{2}, \frac{2y+m}{2}\right) \quad (1)$$

where $I(x,y)$ is intensity of image pixels, x,y – spatial coordinates of image pixels, $w_{m,n}$=[1 4 6 4 1]/16 is a weighting function or smoothing kernel. In our method, we used 2-fold downsampling, which gives a 4-fold increase in the bit depth of each pixel, which is sufficient to obtain high-quality perfusion maps.

Temporal signal filtering. To extract heartbeat-related signals from the video, pixel intensity values are temporally filtered using a digital filter. The infinite impulse response (IIR) filter is chosen due to its simplicity and computational efficiency. Signal filtering is performed using a 2nd order Butterworth band-pass filter in the frequency range of 0.7-3 Hz (heartbeat range 42-180 bpm). Filtered pulsatile signals are obtained in every pixel of the video, using recursive formula:

$$\begin{aligned} Y_n = {} & 0.0586 \cdot G_n - 0.1172 \cdot G_{n-2} + 0.0586 \cdot G_{n-4} \\ & + 2.9918 \cdot Y_{n-1} - 3.5134 \cdot Y_{n-2} \\ & + 1.9522 \cdot Y_{n-3} \end{aligned} \quad (2)$$

where $G_n(x,y)$ is input video frame, $Y_n(x,y)$ is temporally-filtered video frame, n is a number of frame. In each processing step the filtered video frame Y_n is calculated recursively from last 5 frames from the video buffer.

Reference PPG signal. The most accurate method for perfusion map calculation is to use a reference (ground truth) PPG signal which relates to pure cardiac-related signal [20-23]. The reference signal is calculated from those regions where strong heartbeat signal is detected. First, the video frame is divided into rectangular blocks and the pixel values in each block are averaged. The pulsatile signal in each block is calculated in the following way:

$$Z_{i,j,n} = \sum_{m=1}^{M}\sum_{k=1}^{M} Y_{[M(i-1)+k],[M(j-1)+m],n} \quad (3)$$

where Z is a pulsatile signal calculated in the region i,j, $M=16$ is a block size. Next, the signal-to-noise ratio (SNR) is calculated in i,j-th regions, using adapted formula of Haan and Jeanne [16]:

$$SNR = 10log_{10}\frac{\sum_{f=0.7}^{f=3}\Pi(f)|F(f)|^2}{\sum_{f=0.7}^{f=3}(1-\Pi(f))|F(f)|^2} \quad (4)$$

where

$$\Pi(f) = \begin{cases} 1 & |f_0 - f| < 1\ bpm \\ 1 & |2f_0 - f| < 1\ bpm \\ 0 & otherwise \end{cases}$$

where F is the Fourier spectrum of $Z_{i,j}$ signal, f is a heartbeat frequency range, f_0 is a fundamental frequency determined by the maximum peak of Fourier amplitude spectrum in the range of 0.7-3 Hz.

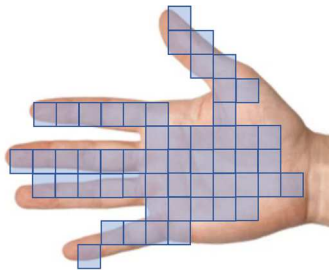

Figure 3: An image of a palm with blue rectangular areas indicating strong pulsatile signal (SNR>0dB).

Finally, the reference signal is formed as a sum of regions where a strong heartbeat signals are detected:

$$R = \sum_{i,j \in S} Z_{i,j} \quad (5)$$

where R is the reference PPG signal, S refers to skin regions where SNR > 0 dB (see Fig. 3).

Blood perfusion map represents the spatially distributed blood perfusion in the skin. It is calculated using the inner product between the signal obtained in each image pixel and the ground-truth reference signal [23]:

$$P(x,y) = \frac{\sum_{n=1}^{N} Y_n(x,y) R_n}{\sqrt{\sum_{n=1}^{N} (Y_n(x,y))^2} \sqrt{\sum_{n=1}^{N} {R_n}^2}} \quad (6)$$

where $P(x,y)$ is a perfusion map which is ranged in [0 1], x,y is a pixel coordinate, $N=250$ is a PPG signal window length in samples (10 s), Y is a pulsatile video signal, R is the reference signal. The following substitution yields:

$$A_1=Y^2,\ A_2=YR,\ A_3=R^2,$$

$$S_1 = \sum_{n=1}^{N} A_{1n} \quad S_2 = \sum_{n=1}^{N} A_{2n} \quad S_3 = \sum_{n=1}^{N} A_{3n}$$

For increasing computing speed, the calculations of sums are performed in the following way: in each n-th captured video frame the total sum of all the elements is calculated, then subtracted the last element and added first element:

$$S_k(x,y,t_n) = \begin{cases} A_k(x,y,t_n) & n = 1 \\ S_k(x,y,t_{n-1}) + A_k(x,y,t_n) & 1 < n \le N \\ S_k(x,y,t_{n-1}) + A_k(x,y,t_n) - A_k(x,y,t_{n-N}) & n > N \end{cases}$$

$$k = 1,2,3 \quad (7)$$

where S_k is a total sum of A_k elements, $N=T*framerate$ is signal buffer length in samples. After the calculating sums S_{123}, the equation (6) can be rewritten in the simpler form:

$$P(x,y,t) = \frac{S_2}{\sqrt{S_1 \cdot S_3}} \quad (8)$$

Equation (8) represents the spatially distributed blood perfusion in the skin, which varies in the time. Perfusion map values range from 0 to 1, therefore normalization is not required. However, in order to separate the pulsating areas of the skin from the background noise, it is necessary to determine the lower threshold of the perfusion map. This can be done by measuring "physiological noise" during provocative tests.

To characterize the normalized intensity of skin perfusion, we introduced the perfusion map density index:

$$PMD(\%) = 100 \frac{\sum_{x \in S} P(\boldsymbol{x})}{\sum_{x \in S} \boldsymbol{x}} \quad (9)$$

where $\boldsymbol{x}$ is a pixel coordinate vector, S refers to skin regions where obtained noticeable perfusion signal, which is defined by threshold: P>0.5.

To increase the speed of real-time calculations (using equations 2 and 7), we use circular buffers. The term "circular buffer" refers to an area in memory used to store incoming data. When the buffer is filled, new data is written starting at the beginning of the buffer and overwriting the old data. The circular buffer only allocates memory when created and operates with memory pointers (matrix indices). This approach offers a noticeable advantage for real-time processing of video data due to its optimization.

2.4. The PPGI software

The PPGI prototype device was supported by dedicated Matlab software developed in the Biophotonics laboratory of IAPS, University of Latvia (author U.Rubins). The software, was implemented on the Microsoft Windows 11 platform, utilizing a laptop computer equipped with an AMD Ryzen 5-series processor and 16 GB of RAM. The graphical user interface (GUI) is depicted in Fig. 4. The GUI comprises two main components: (1) a primary window displaying a video preview image alongside a skin perfusion map, and (2) a control unit for capturing screenshots and annotating specific time moments during various monitoring stages (e.g., baseline, drug administration, anesthesia, etc.). The control unit also enables users to review previously recorded measurements.

Each video measurement is saved in two separate files: 1) RAW video which can be used for offline analysis (e.g. detailed PPG feature analysis), and 2) a video of perfusion maps. RAW videos are stored in a lossless compressed 10-bit format (Motion JPEG-2000, mj2) with a resolution of 640x480 at 25 frames per second. Perfusion map images are stored as 8-bit video sequence (Motion JPEG, mp4) with a resolution of 320x240 at 5 frames per second. The recording duration is solely limited by the available computer storage.

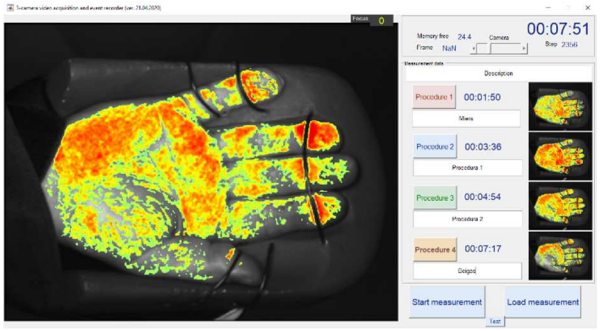

Figure 4: The graphical user interface of PPGI software.

3. Results

The results showed effectiveness of the PPGI system in measuring perfusion changes in a clinical setting, based on an observational study with 7 patients undergoing palm surgery using regional anesthesia (RA). The proposed algorithm's performance is evaluated by comparing the perfusion maps obtained at baseline and after the RA procedures at various time intervals. Additionally, the perfusion map density is introduced as a diagnostic parameter to characterize changes in skin perfusion.

3.1. Blood perfusion maps

The RA procedure (axillary brachial plexus block) is depicted in Fig. 5a. As the local anesthetic is administered in the brachial plexus during the procedure, it affects four different nerves, resulting in subsequent increases in blood circulation in distinct palm areas (dermatomes) [9], as illustrated in Fig. 5b. Perfusion maps (thresholded P>0.5) are combined with palm images in a manner that they appear almost invisible at baseline but become more visible with a progressive increase in perfusion.

Fig. 6 displays palm images merged with thresholded perfusion maps before and after the RA procedures. The images were captured at the following time moments: baseline (0-1 min), 4th, 10th, 15th, and 20th minute after the administration of local anesthetic. The perfusion maps exhibit a noticeable increase in cutaneous microcirculation in the palm immediately following the administration of local anesthetics (5th-20th minutes) for all subjects.

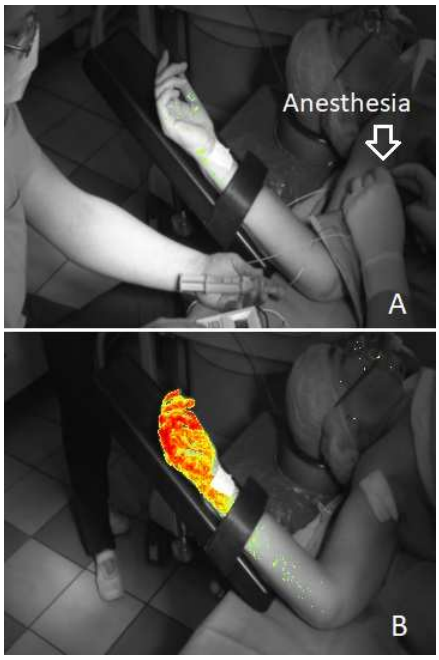

Figure 5: The RA procedure (a) and subsequent increase of blood perfusion map 20 minutes later (b).

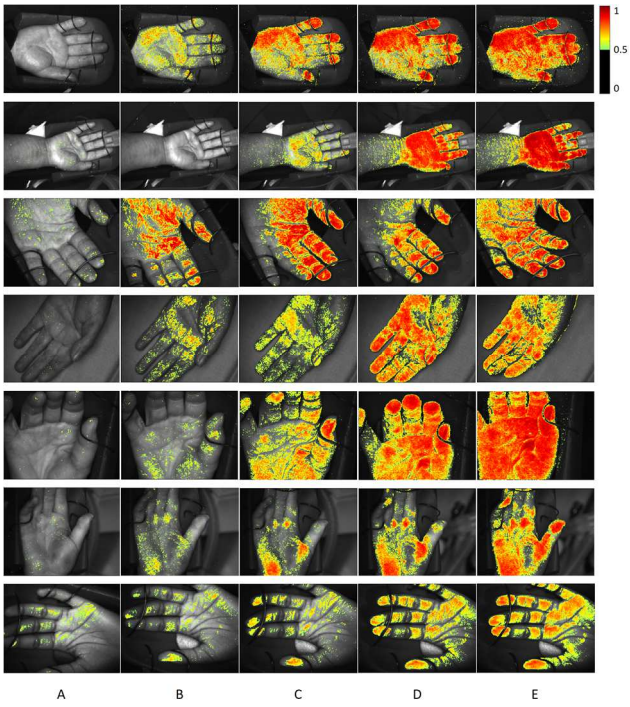

Figure 6: The perfusion maps overlaid with palm's image during 5 stages of measurement of 7 subjects: baseline (0-1 min) (a), 4th, 10th, 15th, and 20th minute after the LA administration (b-e).

3.2. The perfusion map density

To characterize the normalized intensity of skin perfusion, we introduce the perfusion map density (PMD) parameter. Fig. 7 displays the distribution of PMD during baseline and after the RA procedure. The PMD showed increasing median values at different time points: baseline (0-1 minute), and 4, 10, 15, and 20 minutes after the administration of local anesthetic, with values of 53.7%, 57.3%, 64.3%, 70.6%, and 71.1% respectively. These results indicate a significant increase in palm perfusion induced by the local anesthetic.

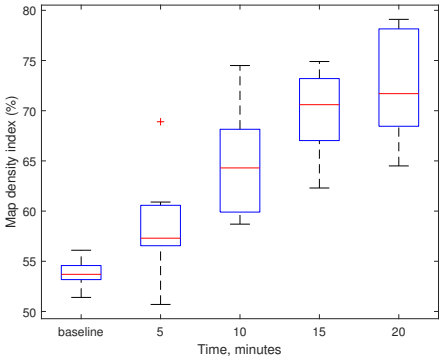

Figure 7: Box plot showing the perfusion map density distribution during the baseline (0-1 minute), and after the LA administration 5, 10, 15 and 20 minute (7 subjects).

4. Discussion

In this study, we introduced an algorithm for real-time blood perfusion mapping with adequate spatial (320x240 pixels) and temporal resolution (0.2s), allowing continuous monitoring of skin blood perfusion. A video resolution of 640x480 pixels is sufficient for visualizing the details of a human palm. On the other hand, the resolution of the perfusion map can be slightly lower due to the diffuse reflectance of green light. Spatial downsampling is known to increase the SNR, and we found that a resolution of 320x240 is adequate for monitoring RA-induced microcirculation changes in different areas of the palm's skin.

PPGI mapping demonstrates its potential in identifying skin areas (dermatomes) affected by local anesthetics. For example, Figure 6 (1st row from top) illustrates how the palm has distinct innervation from the medial and ulnar nerves, resulting in different perfusion patterns in the right and left areas of the palm [9]. In order to exclude "physiological noise" from the PPG signal obtained from palm's skin we used values in the range 0.5-1.0, which was adequate for visualizing perfusion dynamics during the RA provocation. Previously, we tested our developed algorithms for monitoring blood perfusion during various provocations, such as thermal heating of palms [25], liniment application to palm skin [26], application of local anesthetics to gingiva [27], and local anesthetics for patients undergoing palm surgery [7-12]. We focused primarily on palm skin due to its ease of access and suitability for experimentation in both laboratory and clinical settings.

Blood perfusion at any specific skin site depends on multiple physiological factors, such as the patient's circulatory state, vasodilation and vasoconstriction, and the body's reaction to external temperature (neurohumoral control), among others. Additionally, various pathophysiological factors, including patient stress, peripheral arterial disease, and circulatory shock, can cause changes in peripheral perfusion. In our work, we found that a gradual increase in perfusion can be detected using a perfusion map threshold above 50% of maximum intensity. Our introduced Map Perfusion Density has proven to be a reliable indicator of skin blood perfusion during provocation tests.

Rubins et al. previously developed an algorithm for real-time mapping of skin blood perfusion with adequate quality, using Gaussian decomposition and real-time temporal filtering techniques [8]. However, employing a reference PPG signal [20-23] results in a significantly improved quality of PPGI maps. The primary drawback of this approach is its high computational power requirements. Nevertheless, temporal filtering of video (formula 2) and calculation of Pearson's correlation map (formula 6) can be implemented using circular buffers, enabling the implementation of our real-time PPGI map calculation algorithm.

We measured the processing time of proposed algorithm during the measurements, using laptop computer. Real-time processing of each 0.2s buffer (5 frames) included: 1) spatial downsampling (4 ms), 2) temporal filtering (80 ms), 3) reference signal calculation (1 ms), 4) image rendering (10 ms), and 5) video storage (55 ms). During video acquisition, the total processing time does not exceed maximum limit (200ms), which is acceptable for our setup.

The proposed modality's advantages include its simplicity and ease of use in clinical settings. Continuous monitoring of perfusion maps is vital when time is limited, as is often the case before surgical procedures. This greatly facilitates the anesthetist's work. A surgical lamp, present in every operating room, is suitable for illuminating the skin during measurements. This straightforward optical modality, consisting of a surgical lamp, video camera, and computer with processing software, can be further refined.

Future plans include designing a miniature wireless PPGI device for more convenient use in clinical environments. Currently, the system is limited to at-rest monitoring with minimal motion, but image processing functionality can be incorporated in future work, including motion compensation sensing. Furthermore, the PPGI modality can potentially be used to obtain blood perfusion maps from internal tissues using existing cameras attached to an endoscope or a laparoscope with minimal modification.

5. Conclusion

An algorithm for continuous monitoring of cutaneous microcirculation maps with adequate spatial and temporal resolution was proposed in this work. The proposed PPGI system demonstrates its potential in the surgical environment to detect perfusion changes in the skin during regional anesthesia procedures. The algorithm can be implemented on a mid-range laptop computer, and further can be integrated into an embedded wireless system to make it more convenient for medical personnel.

Acknowledgments

This work was supported by the project FLPP-0326 “Multiparametric optical technique for fluid resuscitation and vasopressor therapy guidance in critically ill COVID-19 patients” under the grant agreement lzp-2022/1-0326.

References

[1] Mills, J.L. et al. 2014. The Society for Vascular Surgery Lower Extremity Threatened Limb Classification System: Risk stratification based on Wound, Ischemia, and foot Infection (WIfI). Journal of Vascular Surgery. 59, 1 (Jan. 2014), 220-234.e2. DOI:https://doi.org/10.1016/j.jvs.2013.08.003.

[2] Bailey, M. et al. 2014. Clinical Assessment of Patients with Peripheral Arterial Disease. Seminars in Interventional Radiology. 31, 04 (Nov. 2014), 292–299. DOI:https://doi.org/10.1055/s-0034-1393964.

[3] Bui, D.T. et al. 2007. Free Flap Reexploration: Indications, Treatment, and Outcomes in 1193 Free Flaps. Plastic and Reconstructive Surgery. 119, 7 (Jun. 2007), 2092–2100. DOI:https://doi.org/10.1097/01.prs.0000260598.24376.e1.

[4] den Uil, C.A. et al. 2008. The Microcirculation in Health and Critical Disease. Progress in Cardiovascular Diseases. 51, 2 (Sep. 2008), 161–170. DOI:https://doi.org/10.1016/j.pcad.2008.07.002.

[5] Donati, A. et al. 2013. Towards integrative physiological monitoring of the critically ill: from cardiovascular to microcirculatory and cellular function monitoring at the bedside. Critical Care. 17, S1 (Feb. 2013). DOI:https://doi.org/10.1186/cc11503.

[6] Kara, A. et al. 2016. Monitoring microcirculation in critical illness. Current Opinion in Critical Care. 22, 5 (Oct. 2016), 444–452. DOI:https://doi.org/10.1097/mcc.0000000000000335.

[7] Marcinkevics, Z. et al. 2016. Imaging photoplethysmography for clinical assessment of cutaneous microcirculation at two different depths. Journal of Biomedical Optics. 21, 3 (Mar. 2016), 035005. DOI:https://doi.org/10.1117/1.jbo.21.3.035005.

[8] Rubīns, U. et al. 2016. Photoplethysmography imaging algorithm for continuous monitoring of regional anesthesia. Proceedings of the 14th ACM/IEEE Symposium on Embedded Systems for Real-Time Multimedia. (Oct. 2016). DOI:https://doi.org/10.1145/2993452.2994308.

[9] Rubins, U. et al. 2017. Remote photoplethysmography system for unsupervised monitoring regional anesthesia effectiveness. Biophotonics—Riga 2017. (Dec. 2017). DOI:https://doi.org/10.1117/12.2297158.

[10] Rubins, U. et al. 2017. Simple and convenient remote photoplethysmography system for monitoring regional anesthesia effectiveness. IFMBE Proceedings. (Jun. 2017), 378–381. DOI:https://doi.org/10.1007/978-981-10-5122-7_95.

[11] Rubins, U. et al. 2013. Application of colour magnification technique for revealing skin microcirculation changes under regional anaesthetic input. SPIE Proceedings. (Nov. 2013). DOI:https://doi.org/10.1117/12.2044574.

[12] Rubins, U. et al. 2010. The analysis of blood flow changes under local anesthetic input using non-contact technique. 2010 3rd International Conference on Biomedical Engineering and Informatics. (Oct. 2010). DOI:https://doi.org/10.1109/bmei.2010.5640023.

[13] Poh, M.-Z. et al. 2010. Non-contact, automated cardiac pulse measurements using video imaging and blind source separation. Optics Express. 18, 10 (May 2010), 10762. DOI:https://doi.org/10.1364/oe.18.010762.

[14] Humphreys, K. et al. 2007. Noncontact simultaneous dual wavelength photoplethysmography: A further step toward noncontact pulse oximetry. Review of Scientific Instruments. 78, 4 (2007), 044304. DOI:https://doi.org/10.1063/1.2724789.

[15] Sun, Y. 2011. Motion-compensated noncontact imaging photoplethysmography to monitor cardiorespiratory status during exercise. Journal of Biomedical Optics. 16, 7 (Jul. 2011), 077010. DOI:https://doi.org/10.1117/1.3602852.

[16] de Haan, G. and Jeanne, V. 2013. Robust Pulse Rate From Chrominance-Based rPPG. IEEE Transactions on Biomedical Engineering. 60, 10 (Oct. 2013), 2878–2886. DOI:https://doi.org/10.1109/tbme.2013.2266196.

[17] Xu, S. et al. 2014. Robust efficient estimation of heart rate pulse from video. Biomedical Optics Express. 5, 4 (Mar. 2014), 1124. DOI:https://doi.org/10.1364/boe.5.001124.

[18] Sun, Y. et al. 2011. Motion-compensated noncontact imaging photoplethysmography to monitor cardiorespiratory status during exercise. Journal of Biomedical Optics. 16, 7 (Jul. 2011), 077010. DOI:https://doi.org/10.1117/1.3602852.

[19] Poh, M.-Z. et al. 2011. Advancements in Noncontact, Multiparameter Physiological Measurements Using a Webcam. IEEE Transactions on Biomedical Engineering. 58, 1 (Jan. 2011), 7–11. DOI:https://doi.org/10.1109/tbme.2010.2086456.

[20] Kumar, M. et al. 2020. PulseCam: a camera-based, motion-robust and highly sensitive blood perfusion imaging modality. Scientific Reports. 10, 1 (Mar. 2020). DOI:https://doi.org/10.1038/s41598-020-61576-0.

[21] Kamshilin, A.A. et al. 2011. Photoplethysmographic imaging of high spatial resolution. Biomedical Optics Express. 2, 4 (Mar. 2011), 996. DOI:https://doi.org/10.1364/boe.2.000996.

[22] Kamshilin, A.A. et al. 2013. Variability of Microcirculation Detected by Blood Pulsation Imaging. PLoS ONE. 8, 2 (Feb. 2013), e57117. DOI:https://doi.org/10.1371/journal.pone.0057117.

[23] Amelard, R. et al. 2017. Non-contact hemodynamic imaging reveals the jugular venous pulse waveform. Scientific Reports. 7, 1 (Jan. 2017). DOI:https://doi.org/10.1038/srep40150.

[24] Verkruysse, W. et al. 2008. Remote plethysmographic imaging using ambient light. Optics Express. 16, 26 (Dec. 2008), 21434. DOI:https://doi.org/10.1364/oe.16.021434.

[25] Marcinkevics, Z. et al. 2021. Remote Photoplethysmography for Evaluation of Cutaneous Sensory Nerve Fiber Function. Sensors. 21, 4 (Feb. 2021), 1272. DOI:https://doi.org/10.3390/s21041272.

[26] Rubins, U. and Marcinkevics, Z. 2017. Comparison of remote photoplethysmography signals acquired by ultra-low noise camera and conventional camera during physiological tests. Clinical and Preclinical Optical Diagnostics. (Jul. 2017). DOI:https://doi.org/10.1117/12.2284657.

[27] Rubins, U. et al. 2019. Remote photoplethysmography for assessment of oral mucosa. Clinical and Preclinical Optical Diagnostics II. (Jul. 2019). DOI:https://doi.org/10.1117/12.2526979.

[28] Andelson, E.H. et al. 1984. Pyramid methods in image processing. RCA Engineer 29 (6); 33-41.